DETECTION OF THE CORNER STRUCTURES IN 3D ARRAYS USING SCALABLE MASKS

I.G. KAZANTSEV, B.O. MUKHAMETZHANOVA, K.T. ISKAKOV

Abstract. Scalable masks for the selection of angular structures in three-dimensional (3D) digital images are considered, which are used in processing with a 3D window sliding over the image and convolved with image fragments. The model of scalable 3D mask was developed based on expanding smaller mask along its sides and edges. In this case, the submatrices remain unchanged, and new elements are added by repeating the elements of the submatrix, preserving the structure of the corner. This approach helps to design the hierarchical computations of 3D data.

Keywords: image processing, sliding window, scalable mask, corner detection.

1. INTRODUCTION

The new masks are considered for detecting corners in three-dimensional images to be used in the traditional method [1] of sliding windows. Interest in creating some noise-resistant and efficient corner detection algorithms has existed for decades, and the sources of the methods being created are many areas of science: from image processing and optics to differential and integral geometry [2], [3], [4]. Recent surveys can be found in [5], [6], [7], A separate topical problem is face recognition,

where the method of local binary patterns has a particular application. This approach is based on a variant of directional derivatives and known as the Kirsch differentiating masks [9], [10]. The mathematical aspects of computer vision and regularization of the solution of the inverse problems of image processing by using a priori information about sparsity of the corner points on image objects are investigated in [11], [12].

The vertices of corner structures, or corner points, are an important local feature of the image and belong to the class of the so-called dominant, characteristic, singular, or points of interest, etc. Corners are invariant to rotation and changes in the lighting conditions. They are used as reference points in the work with stereopairs, as features in face recognition (for example, the corners of the eyes), fingerprints and letters in the texts, 3D reconstruction from a collection of affine views, and tracking. Interesting field of applications of the detection of corners in 3D arrays emerges in recent years with wide using the depth cameras and other stereo vision sensors providing three-dimensional information [13], [14], [15]. Important applications include camera calibration, robot navigation and machine vision, image matching, and pattern recognition. In our recent work we have derived scalable masks for detecting the corners in two-dimensional images [16]. The current paper considers extension of this approach onto similar masks for finding corners in images for use on three-dimensional meshes.

The article is structured as follows. Section 2 shows examples of 2D corner masks. Section 3 outlines the principles for constructing scalable 3D masks. Section 4 presents algorithms for selecting corners. The article ends with conclusions.

2. EXAMPLES OF 2D SCALABLE MASKS

Depending on the applications, the corner itself is also called the vertex of the angle, that is, a separate point, and a less local object, including, in addition to the vertex, also the rays propagating from it, as well as the entire angular structure. In the processing of three-dimensional 3D images, the sides that make up the border of the corner (generally, a polytop) are added to the straight lines (edges), in which the dominant changes in brightness are visually observed, characterizing the difference between one area of the image (corner) from another (background). One of the common approaches to finding corners consists in boundary detection and binarization, and subsequent detection procedures on a binary analogue of an image. This method is based on the studying the brightness of the image in the vicinity of a point for the equality to zero of the second derivative and a change in the sign in the direction normal to the boundary.

In this paper we consider the group of algorithms that does not perform edge selection and binarization, but works directly with a grayscale image, scanning its elements with a local neighborhood and calculating the correlation of a snapshot fragment with a mask programming the angular structure model. It is assumed that the inner region of the corner is approximately a plateau. The size of the mask is uneven; when the image is scanned, the central element of the mask is placed in the center of the examined image fragment. For each element of the image, the values of the convolution of the fragment and the mask are calculated for its various rotations about the central element. The maximum absolute value of these is retained as a measure of the presence of a corner at a point.

Many differentiating masks, or discrete kernels of two-dimensional convolution are known [1]. Among such schemes for constructing masks, the Kirsch mask, which simulates oriented boundaries, stands out:

$$(1) \quad K^1 = \begin{array}{|c|c|c|} \hline 5 & 5 & 5 \\ \hline -3 & 0 & -3 \\ \hline -3 & -3 & -3 \\ \hline \end{array}, \; K^2 = \begin{array}{|c|c|c|} \hline -3 & 5 & 5 \\ \hline -3 & 0 & 5 \\ \hline -3 & -3 & -3 \\ \hline \end{array}, \; K^3 = \begin{array}{|c|c|c|} \hline -3 & -3 & 5 \\ \hline -3 & 0 & 5 \\ \hline -3 & -3 & 5 \\ \hline \end{array}, \ldots, K^8,$$

where three of eight rotated versions are shown. The considered detectors have property of non-scalability, which creates problems for organizing fast computations. For example, scanned data with a 3×3 mask is problematic to use in calculations with large masks. Calculations with masks of sequentially increasing sizes contain information about the linear and areal parameters and the moment of the corner transition to the background area. In comparison with the Kirsh masks (1), a scalable masks are obtained under the assumption that the border between the corner structure and the background passes inside a certain pixel through its center, and not between two adjacent pixels along their sides or edges. Scalable 3×3 masks are shown for comparison with (1):

$$(2) \quad W_2^1 = \begin{array}{|c|c|c|} \hline 1 & 3 & 1 \\ \hline -1 & 0 & -1 \\ \hline -1 & -1 & -1 \\ \hline \end{array}, W_2^2 = \begin{array}{|c|c|c|} \hline -1 & 1 & 3 \\ \hline -1 & 0 & 1 \\ \hline -1 & -1 & -1 \\ \hline \end{array}, W_2^3 = \begin{array}{|c|c|c|} \hline -1 & -1 & 1 \\ \hline -1 & 0 & 3 \\ \hline -1 & -1 & 1 \\ \hline \end{array}, \ldots, W_2^8,$$

where W_n^r denotes the $r-$th rotated version of the mask $(r = 1, \ldots, R)$ of $N \times N$ size with $N = 2n - 1$. Let us outline in short the main priciples of scalable masks modeling. Firstly, the matrix is introduced with a possibility of expanding it to larger sizes. The vertex (0) is centered in the middle of the mask, the corner edges $(a-$s) embrace the angular body $(c-$s):

$$(3) \quad W_3^1 = \begin{array}{|c|c|c|c|c|} \hline a & c & c & c & a \\ \hline d & a & c & a & d \\ \hline & d & 0 & d & \\ \hline & & d & & \\ \hline & & & & \\ \hline \end{array}, W_3^2 = \begin{array}{|c|c|c|c|c|} \hline d & a & c & c & \\ \hline d & a & c & c & \\ \hline d & 0 & a & a & \\ \hline d & d & d & d & \\ \hline & & & & \\ \hline \end{array}, W_3^3 = \begin{array}{|c|c|c|c|c|} \hline & & & & 1 \\ \hline & & & 1 & 3 \\ \hline & 0 & 3 & 3 & \\ \hline & & 1 & 3 & \\ \hline & & & & 1 \\ \hline \end{array}, \ldots,$$

where empty cells are assigned with background values $(d-$s). We need some definitions.

Definition 1. *The matrices W_n of the odd size $(2n - 1)^2$, $n = 2, \ldots$ with zero central entry $W_n(n, n) = 0$ and non central entries $a, c,$ and d are called scalable masks of angular structures provided the following conditions are satisfied:*

   (i) *A set of entries $A_n = \{a\}$ simulating the sides of the corner consists of two digital halflines starting at zero point $O = \{0\}$ and spreading from it either along a column and a row, or along a column/row and one of the four diagonals, or along two diagonals.*

   (ii) *A set of entries $C_n = \{c\}$ of the matrix enclosed by the sides of the corner is called a body of the corner.*

   (iii) *The remaining entries form a set $D_n = W_n \setminus (O_n \cup A_n \cup Cn)$, called a background.*

The model of the corner mask includes the principle of self-similarity consisting in the fact that, as the number n increases, the values a of the corner sides are extended along a given propagation line (rows, columns, diagonals). Moreover, the

(a) (b)
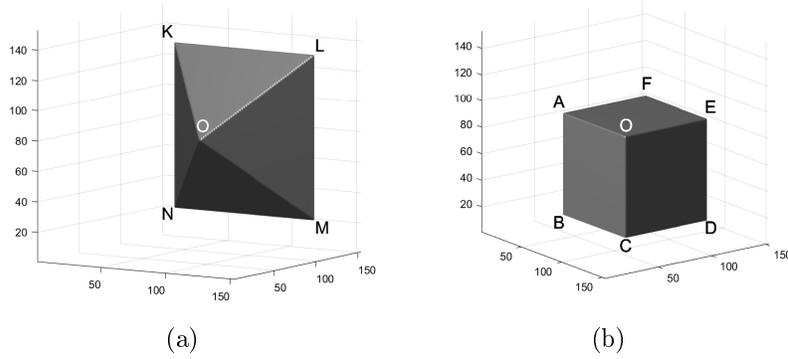
FIG. 1. A general view of 3D arrays of two corner models with O as the corner vertex at the array center. (a) The frustum-wise corner $OKLMN$. (b) The octant-wise corner $OABCDEF$.

values c of the internal elements of the corner body are spreading from the center of the mask to its periphery, whereas the background values d fill the mask region complementary to the corner elements. The central entry of the mask is chosen to be zero, as well as the sum of all mask entries. This explains the differentiating effect on the image, produced by convolution with a sliding mask of this type. Denote by $|A_n|$, $|C_n|$, $|D_n|$, and $|O_n| \equiv 1$ the number of mask entries with the values a, c, d, and 0, respectively. The number of all mask entries W_n (for convenience, the superscripts are omitted) equals $|W_n| = (2n - 1)^2$. Let us calculate the values $|A_n|$, $|C_n|$, $|D_n|$ and write down the differential mask condition as follows. We can express the values $|A_n|$, $|C_n|$, $|D_n|$ in the general form

(4) $$|A_n| = 2(n - 1),\ |C_n| = (n - 1)^2,\ |D_n| = (n - 1)(3n - 1),$$

and write down the differential mask condition as follows

(5) $$|A_n|\, a + |C_n|\, c + |D_n|\, d = 0.$$

Then we arrive at the differential condition (5) in the form:

(6) $$2\, a + (n - 1)\, c + (3n - 1)\, d = 0.$$

Due to the scalability of matrices, we have another similar equation for an arbitrary m

(7) $$2\, a + (m - 1)\, c + (3m - 1)\, d = 0,$$

and, subtracting (7) from (6), obtain

(8) $$c + 3d = 0.$$

Then we substitute $c = -3d$ into (6) and find the solution in terms of d:

(9) $$(a, c, d) = (-d, -3d, d) = d(-1, -3, 1) = -d(1, 3, -1).$$

Relatively prime weights $(a, c, d) = (1, 3, -1)$ constitute a scalable mask of the angles of 90 degrees. Scalable masks, their derivation and numerical experiments with test 2D images are given in [16]. In what follows we try to design a 3D masks that have similar constructive properties of scalability.

3. THE 3D SCALABLE MASKS

In the case of a three-dimensional array W_n of $(2n-1)^3$ size, we focus on the two models of angular structures: frustums (pyramids) (Fig. 1 (a)) and octants (Fig. 1 (b)) with a vertex at the center (n, n, n) of the 3D array. The cube has six frustums and eight octants by the number of cube sides and vertices, respectively. The frustums and octants have opening solid angles $4\pi/6$ and $4\pi/8$, respectively. We should note that further central sectioning of the frustum corner $OKLMN$ leads to finer angular structure, the pyramid $OKLM$, for example, with the solid angle $OKLM$. In this paper we do not consider such a decomposition into subangles. Let us summarize the principles of designing scalable masks from the two-dimensional case to the three-dimensional one with the following definitions.

Definition 2. *The matrices W_n of the size $(2n-1) \times (2n-1) \times (2n-1)$, $n = 2, \ldots$, with a zero central entry $W_n(n, n) = 0$ and non central entries a, b, c and d are called scalable masks of angular structures provided the following conditions are satisfied for all $n = 2, \ldots$:*

  (i) *A set of entries $A_n = \{a\}$ simulating the edges of the corner consists of digital halflines starting at zero point $O = \{0\}$ and spreading from it either along coordinates, or along a coordinate(s) and a diagonal(s), or along diagonals.*

  (ii) *A set of entries $B_n = \{b\}$ of the matrix "enclosed" by the edges of the corner is called a side of the corner.*

  (iii) *A set of entries $C_n = \{c\}$ of the matrix "enclosed" by the edges and the sides of the corner is called a body of the corner.*

  (iiii) *The remaining entries form a set $D_n = W_n \setminus (O_n \cup A_n \cup B_n \cup C_n)$, are called a background.*

Denote by $|A_n|$, $|B_n|$, $|C_n|$, $|D_n|$ and $|O_n| \equiv 1$ the number of mask entries with the values a, b, c, d and 0, respectively. The number of all mask entries $|W_n|$ equals $|W_n| = (2n-1)^3$. The differential mask condition in the general form is the following:

$$(10) \qquad\qquad |A_n|a + |B_n|b + |C_n|c + |D_n|d = 0.$$

3.1. Frustum Corners. One of the six rotated versions of a frustum corner is shown in Fig. 1 (a). The frustum corner $OKLMN$ has four edges OK, OL, OM, ON and four sides OKL, OLM, OMN, ONK.

The weights a, b, c within the frustum corner model $OKLMN$ are illustrated in Fig. 2 (a), slice $QPRS$. Examples of slices are shown in Fig. 2 (b),(c) for $(n = 2, N = 3)$ and $(n = 3, N = 5)$, respectively. We enumerate the slices according to the number n, the second and the third slices of the corner are shown in Fig. 2 (b),(c), respectively. We supply the reader with other graphical explanatory pictures of the frustum corner structure in Fig. 3.

Omitting the details of derivation, we calculate the entities $|A_n|$, $|B_n|$, $|C_n|$, $|D_n|$ in equation (10):

$$(11) \qquad |A_n| = 4(n-1), \;\; |B_n| = 4(n-1)^2, \;\; |C_n| = \frac{(n-1)(2n-1)(2n-3)}{3}.$$

Then

$$(12) \qquad |D_n| = |W_n| - |A_n| - |B_n| - |C_n| - |O_n| = \frac{(n-1)(2n-1)(10n-1)}{3}.$$

(a)   (b)   (c)
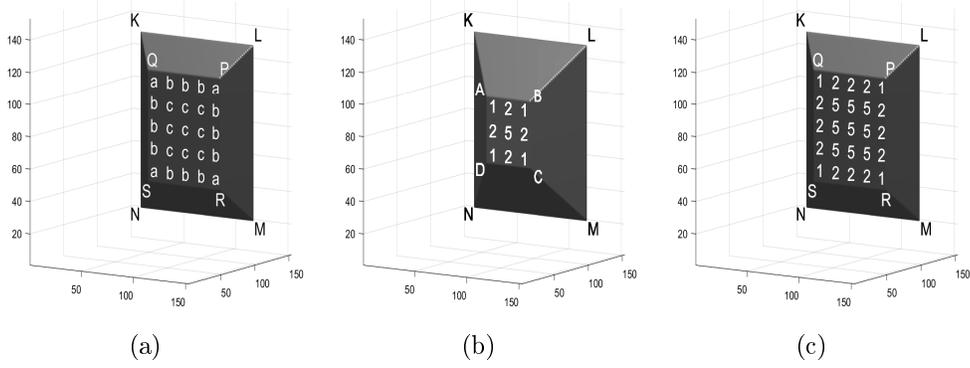
FIG. 2. Visualization of several slices of the frustum corner model with scalable weights. (a) General notations within the frustum corner: a stands for the frustum edges voxels except the vertex O, b is the weight for frustum sides except edges, c is the weight of the corner body. (b) The slice $ABCD$ with a part of the 3^3 mask. (c) The slice $QPRS$ with a part of the 5^3 mask.

Proposition 1. *The values of the frustum masks are $(a, b, c, d) = (1, 2, 5, -1)$.*

Proof. Calculating $|A_n|$, $|B_n|$, $|C_n|$, $|D_n|$ using (11), (12), with values $n = 2, 3, 4, 5$ and inserting them into (10), we arrive at the system

$$(13) \qquad \begin{pmatrix} 4 & 4 & 1 & 17 \\ 8 & 16 & 10 & 90 \\ 12 & 36 & 35 & 259 \\ 16 & 64 & 84 & 564 \end{pmatrix} \begin{pmatrix} a \\ b \\ c \\ d \end{pmatrix} = \begin{pmatrix} 0 \\ 0 \\ 0 \\ 0 \end{pmatrix}.$$

Application of the Gauss-Jordan elimination technique [17] gives us

$$(14) \qquad \begin{pmatrix} 1 & 0 & 0 & 1 \\ 0 & 1 & 0 & 2 \\ 0 & 0 & 1 & 5 \\ 0 & 0 & 0 & 0 \end{pmatrix} \begin{pmatrix} a \\ b \\ c \\ d \end{pmatrix} = \begin{pmatrix} 0 \\ 0 \\ 0 \\ 0 \end{pmatrix}.$$

We find a solution in terms of d:

$$(15) \qquad (a, b, c, d) = (-d, -2d, -5d, d) = -d(1, 2, 5, -1).$$

Relatively prime weights $(a, b, c, d) = (1, 2, 5, -1)$ constitute a scalable mask of 3D frustum corners. The proof is completed. □

3.2. Octant Corners. One of the eight rotated versions of the octant corner is shown in Fig. 1 (b). The octant corner $OAFEDCB$ has three edges OA, OE, OC, and three sides $OAFE$, $OEDC$, $OCBA$. The weights a, b, c within the octant corner model $OAFEDCB$ can be seen in Fig. 4 (a), the slice $GHIJ$. Examples of sides and slices of the octant corner are shown in Fig. 4 (b),(c) for $n = 4$ and $N = 7$ respectively.
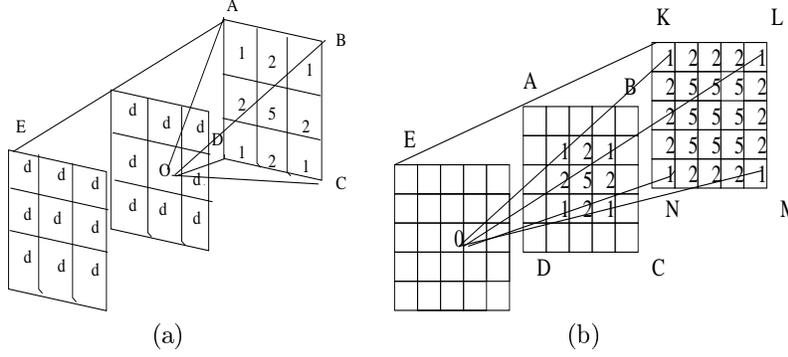
FIG. 3. Examples of the frustum corner matrices of $N \times N \times N$ size. (a) $N = 3$, frustum $OABCD$. (b) $N = 5$, frustum $OKLMN$.

Omitting the details of derivation, we calculate the entities $|A_n|$, $|B_n|$, $|C_n|$, $|D_n|$ for the octant corner model in equation (10):

(16) $$|A_n| = 3(n - 1), \ |B_n| = 3(n - 1)^2, \ |C_n| = (n - 1)^3.$$

Then

(17) $$|D_n| = |W_n| - |A_n| - |B_n| - |C_n| - |O_n| = (2n - 1)^3 - n^3.$$

Proposition 2. *The weights of the octant corners are* $(a, b, c, d) = (1, 3, 7, -1)$.

Proof. Calculating $|A_n|$, $|B_n|$, $|C_n|$, $|D_n|$ using (16), (17), with values $n = 2, 3, 4, 5$ and inserting them into (10), we arrive at the system

(18) $$\begin{pmatrix} 3 & 3 & 1 & 19 \\ 6 & 12 & 8 & 98 \\ 9 & 27 & 27 & 279 \\ 12 & 48 & 64 & 604 \end{pmatrix} \begin{pmatrix} a \\ b \\ c \\ d \end{pmatrix} = \begin{pmatrix} 0 \\ 0 \\ 0 \\ 0 \end{pmatrix}.$$

Application of the Gauss-Jordan elimination technique reduces system (18):

(19) $$\begin{pmatrix} 1 & 0 & 0 & 1 \\ 0 & 1 & 0 & 3 \\ 0 & 0 & 1 & 7 \\ 0 & 0 & 0 & 0 \end{pmatrix} \begin{pmatrix} a \\ b \\ c \\ d \end{pmatrix} = \begin{pmatrix} 0 \\ 0 \\ 0 \\ 0 \end{pmatrix}.$$

We find a solution in terms of d:

(20) $$(a, b, c, d) = (-d, -3d, -7d, d) = -d(1, 3, 7, -1).$$

Relatively prime weights $(a, b, c, d) = (1, 3, 7, -1)$ constitute a scalable mask of 3D octant corners. The proof is completed. $\qquad\square$

4. COMPUTATIONAL SCHEME OF CORNER DETECTION

Let F denote the part of the larger image f, (i.e., a fragment) of $N \times N$ size (in 2D case) and $N \times N \times N$ (in 3D case), on which the sliding window W_n ($N = 2n - 1$) of the same size as F has stopped. A measure of similarity of a fragment and a
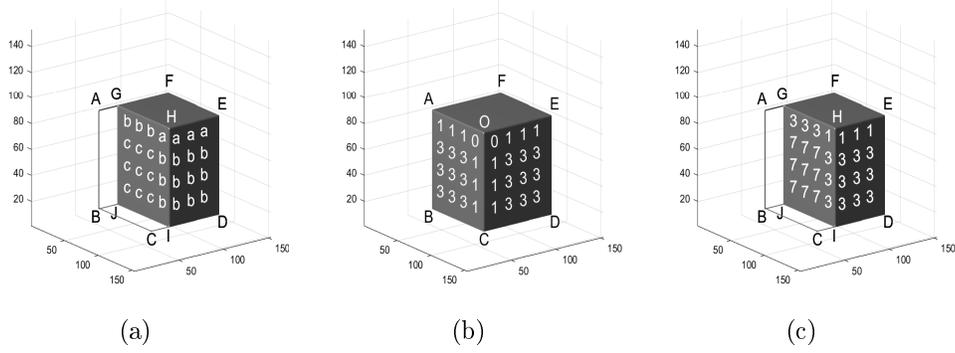
Fig. 4. Visualization of the octant corner model. (a) The notations within the octant corner, the slice $GHIJ$: a stands for the frustum edges (OE, OC, OA) voxels except vertex O (not shown), b is the weight for frustum sides except edges, c is the weight of the corner body. (b) Slices $OCBA$, $OAFE$ and $OEDC$ are the sides of corner $OAFEDCB$ within the 7^3 mask. (c) Slice $GHIJ$ is a part of corner within the 7^3 mask.

rotational version W_n^r, $r = 1, \ldots, R$ of the mask W_n can be obtained from the well-known identity

$$(21) \qquad \|F - W_n^r\|^2 = \|F\|^2 - 2\langle F, W_n^r \rangle + \|W_n^r\|^2$$

in the chosen norm of the Hilbert space. It follows from this relation that the fragment F is best approximated by the ideal corner W by finding a maximum of the inner product $\langle F, W_n^r \rangle$, due to $\|W_n^r\|^2 = const$. Then the criterion for detecting a corner can be formulated in the form

$$(22) \qquad Q = \max_{r,n} \langle F, W_n^r \rangle.$$

When the fragment F of N^3 size, centered in the pixel with the current coordinates (i, j, k) moves over the image field f, the scalar product of the fragment F with the matrix of the mask W_n^r, $r = 1, \ldots, R$ is computed:

$$(23) \qquad u_n^r(i, j, k) = \langle F, W_n^r \rangle.$$

We calculate the image of the maximum responses among the rotations

$$(24) \qquad U_n^R(i, j, k) = \max_{r=1,\ldots,R} |u_n^r(i, j, k)|.$$

It is expected that the maximum response occurs with the orientation of the mask that is in the best agreement with the rotation of the corner observed in the fragment. The spatial extension of the corner along its sides can be evaluated by varying another parameter, the mask size n. To this end, we choose the integer M as an estimate of the maximum size of the corner encountered, and calculate the image of maximum responses to the mask growth:

$$(25) \qquad V_M^R(i, j, k) = \max_{n=1,\ldots,M} U_n^R(i, j, k).$$

It is assumed that, with increasing the tested corner size, the response grows to the limits of the corner extension, and upon reaching them, some saturation of the response or a more complex event occurs due to the mask capturing the non-corner areas. While studying the visual properties of the image V_M^R, we observe a version of the original image with increased brightness at the corner points.

Now the corner points themselves can be obtained by introducing a classification threshold, which leaves the significant, or dominant, points in the image. Many threshold search methods are available, including the dynamic, locally adapted thresholds [1]. The problem of normalization of the detection criterion remains challenging because the corners in images have different intensities. As a consequence, the scatter in the range of the response values V_M^R in (25) forms the basis for the terms of "strong" and "weak" corners. One of the options for selecting corners is to choose a given number of strong (weak) corners. It appears that the solution to these problems requires a complete description of the corner features in the domain of the parameters (r, n, M) and time-consuming operations with local extremes.

It is known that some information is lost while performing the algorithm steps in (23)–(25). The hierarchical scalable approach we are developing suggests preserving results at these stages as features and examining the data as a whole, not only by the coordinate search for maxima over r and n. The algorithm allows us to sort the corner structures and then to analyze them according to various characteristics, for example, in terms of distributions of orientations of the corners.

The sum of the entries of the mask boundary equals zero. It means that, in addition to the property of masks to have a differentiating character in general (the sum of the entries is zero), the mask boundary also possesses this property. When the size of the growing mask exceeds the corner region and the boundaries of the mask reach the non-corner areas of the image with arbitrary values, the contribution of these regions to the criterion values can change, and a discord is observed. It is difficult to choose in advance the size of a mask in proportion to the size of the desired corner structures, and we encounter the problem of detecting the moment [18], [19] of a significant event (jump, disorder, saturation, etc.) and changing the criterion.

5. Conclusion

We have presented the matrices of masks for detecting the corners, convenient for constructing scalable detectors. The structures potentially identified by the approach proposed include the cones in the form of octants and frustums with vertices at the center of a three-dimensional array. These constructions do not require a sliding window to re-pass the image array, since combination takes place at the next level of the scale or the hierarchy, based on the basic procedures of the lower level, operating with borders. The method can be used along with the traditional masks for analyzing images, but without restrictions on the choice of the size of the masks. We expect that computer time would be saved using the fast Fourier transform in multiple computations of convolutions. Comprehensive numerical experiments and comparative studies including other efficient corner detection algoritms are the subject of the near future research.

References

[1] R.C. Gonzalez, R.E. Woods, *Digital Image Processing*, Pearson, NY, 2018.

[2] T. Tuytelaars, K. Mikolajczyk, *Local Invariant Feature Detectors: A Survey,* Foundations and Trends in Computer Graphics and Vision, **3**:3 (2008), 177—280.

[3] R. Reisenhofer, E.J. King, *Edge, Ridge, and Blob Detection with Symmetric Molecules,* SIAM J. Imaging Sci., **12** (2019):4, 1585–1626.

[4] T. Lindeberg, *Spatio-temporal scale selection in video data,* J. Math. Imaging Vis., **60**:4 (2018), 525—562. Zbl 1420.94015

[5] W. Zhang, C. Sun, T. Breckon, N. Alshammari, *Discrete curvature representations for noise robust image corner detection,* IEEE Trans. Image Process., **28**:9 (2019), 4444–4459.

[6] A. Dutta, A. Kar, B.N. Chatterji, *Corner detection algorithms for digital images in last three decades,* IETE Technical Review, **25**:3 (2008), 123–133.

[7] J. Chen, L. Zou, J. Zhang, L. Dou, *The Comparison and Application of Corner Detection Algorithms,* Journal of Multimedia, **4** (2009), 435–441.

[8] E. Rosten, R. Porte, T. Drummond, *Faster and Better: A Machine Learning Approach to Corner Detection,* IEEE Transactions on Pattern Analysis and Machine Intelligence, **32**:1 (2010), 105–119.

[9] B.H. Shekar, K.P. Uma, *Kirsch directional derivatives based shot boundary detection: an efficient and accurate method,* Procedia Computer Science, **58** (2015), 565–571.

[10] M. Pietikainen, G. Zhao, *Two decades of local binary patterns: A survey,* Advances in Independent Component Analysis and Learning Machines. Academic Press, 2015, Chapter 9., 175–210.

[11] A. Buades, R. Grompone von Gioi, J. Navarro, *Joint contours, corner and T-junction detection: an approach inspired by the mammal visual system,* J. Math. Imaging Vision, **60**:4 (2018), 341—354. Zbl 1433.68507

[12] H. Liu, S. Tan, *Image regularizations based on the sparsity of corner points*, IEEE Trans. Image Process., **28**:1 (2019), 72–87. Zbl 1409.94373

[13] J. Ruiz-Alzola, R. Kikinis, C.-F. Westin, *Detection of point landmarks in multidimensional tensor data,* Signal Process., **81**:10 (2001), 2243–2247.

[14] I. Sipiran, B. Bustos, *Harris 3D: a robust extension of the Harris operator for interest point detection on 3D meshes*, Visual Computer, **27**:11 (2011), 963–976.

[15] L.E. Ortiz, E.V. Cabrera, L.M. Gonçalves, *Depth data error modeling of the ZED 3D Vision sensor from stereolabs*, Electronic Letters on Computer Vision and Image Analysis, **17**:1 (2018), 1–15.

[16] I.G. Kazantsev, B. O. Mukhametzhanova, K.T. Iskakov, T. Mirgalikyzy, *Detection of the corner structures in images by scalable masks*, J. Appl. Ind. Math., **14** (2020), 73–84.

[17] G.H. Golub, C.F. Van Loan, *Matrix Computations*, Johns Hopkins Univ. Press, Baltimore, 1996. Zbl 0865.65009

[18] A.N. Shiryaev, *Stochastic disorder problems*, Probability Theory and Stochastic Modelling, **93**, Springer, Cham, 2019. Zbl 1426.93002

[19] A.A. Borovkov. *On estimation of parameters in the case of discontinuous densities,* Theory Probab. Appl. **63**:2 (2918), 169–192. Zbl 1404.62024

Ivan G. Kazantsev
Institute of Computational Mathematics and Mathematical Geophysics,
6, Akademic Lavrentiev ave.,
Novosibirsk, 630090, Russia
Email address: kazantsev.ivan6@gmail.com

Bigul O. Mukhametzhanova
L.N. Gumilyov Eurasian National University,
2, Satpayev str.,
Nur-Sultan, 010008, Kazakhstan
Email address: grek79@mail.ru

Kazizat T. Iskakov
L. N. Gumilyov Eurasian National University,
2, Satpayev str.,
Nur-Sultan 010008, Kazakhstan
Email address: kazizat@mail.ru